Nanoscale Advances

ROYAL SOCIETY OF CHEMISTRY

PAPER

View Article Online
View Journal | View Issue

Cite this: *Nanoscale Adv.*, 2023, **5**, 1776

Rapid controllable synthesis of branched Au superparticles: formation mechanism of toggling the growth mode and their applications in optical broadband absorption†

Shichuan Zhong, ‡[a] Lifeng Hang, ‡[b] Lulu Wen,[a] Tao Zhang, [ac] An Cao,[a] Pan Zeng,[a] Hanlin Zhang,[a] Dilong Liu, [a] Weiping Cai [a] and Yue Li *[a]

We develop a tunable, ultrafast (5 seconds), and mass-producible seed-mediated synthesis method to prepare branched Au superparticles consisting of multiple small Au island-like nanoparticles by a wet chemical route. We reveal and confirm the toggling formation mechanism of Au superparticles between the Frank–van der Merwe (FM) growth mode and the Volmer–Weber (VW) growth mode. The key factor of this special structure is the frequent toggling between the FM (layer by layer) growth mode and the VW (island) growth mode induced by 3-aminophenol, which is continuously absorbed on the surface of newborn Au nanoparticles, leading to a relatively high surface energy during the overall synthesis process, thus achieving an island on island growth. Such Au superparticles demonstrate broadband absorption from visible to near-infrared regions due to their multiple plasmonic coupling and hence they have important applications in sensors, photothermal conversion and therapy, *etc.* We also exhibit the excellent properties of Au superparticles with different morphologies, such as NIR-II photothermal conversion and therapy and SERS detection. The photothermal conversion efficiency under 1064 nm laser irradiation was calculated to be as high as 62.6% and they exhibit robust photothermal therapy efficiency. This work provides insight into the growth mechanism of plasmonic superparticles and develops a broadband absorption material for highly efficient optical applications.

Received 4th January 2023
Accepted 14th February 2023

DOI: 10.1039/d3na00008g

rsc.li/nanoscale-advances

Introduction

In the past two decades, gold nanorods (Au NRs) as typical near-infrared (NIR) resonant plasmonic materials have been widely applied in many optical sensing fields due to their uniform shape and tunable aspect ratio as well as remarkable field enhancement effect,[1] such as surface-enhanced Raman spectroscopy (SERS), *in vivo* photoacoustic imaging and photothermal therapy, and NIR chiral optics.[2–5] However, their NIR extinction is related to the longitudinal plasmonic resonant mode triggered by longitudinally polarized light, leading to its dependence on the polarization-light direction.[6] Therefore, Au NRs have a relatively low NIR optical utilization in most application environments because of their random orientation.

In contrast, Au superparticles (superparticles: size- and shape-controlled Au nanoparticle assemblies) with 3D structures are independent of light polarization and possess a high NIR optical utilization due to their multiple couplings in the 3D orientation.[7,8] However, most of the Au superparticles were obtained by self-assembly and their stability was not good. As a result, their practical applications were seriously restricted.[9–12] In contrast, the stability of superparticles fabricated by wet chemical methods proved to be relatively high,[13] but their direct synthesis still remains a challenge. Recently, Yin *et al.* reported a seed-mediated growth method to directly synthesize Au superparticles with broadband absorption in the NIR region by the reduction of chloroauric acid using dopamine under nitrogen flow in 6 hours and these emerging NIR plasmonic materials possessed an ultra-high photothermal conversion efficiency both experimentally and theoretically.[14]

However, for Au superparticles as a kind of new material, it is not enough to rely only on their high NIR optical utilization to replace the positions of Au NRs in some sensing regions. Crucially, the tunable optical properties of Au NRs for a variety of applications are their main competitive factors.[1] Since the

[a]*Key Lab of Materials Physics, Anhui Key Lab of Nanomaterials and Nanotechnology, Institute of Solid State Physics, Hefei Institutes of Physical Science, Chinese Academy of Sciences, Hefei 230031, Anhui, P. R. China. E-mail: yueli@issp.ac.cn*

[b]*The Department of Medical Imaging, Guangdong Second Provincial General Hospital, Guangzhou 518037, P. R. China*

[c]*School of Physical and Mathematical Sciences, Nanyang Technological University, 21 Nanyang Link, Singapore 637371, Singapore*

† Electronic supplementary information (ESI) available. See DOI: https://doi.org/10.1039/d3na00008g

‡ These authors contributed equally to this work.

optical properties of Au nanoparticles depend on their morphology and scale, therefore, it is important to gain an in-depth understanding of the growth mechanism of branched Au superparticles for accurate morphological regulation of this emerging material. However, it is difficult to directly elucidate the growth mechanism of this branched structure in previous studies because of multiple surfactants and complicated fabrication processes. Therefore, a facile, rapid, and mass-producible synthetic method is not only a requirement of practical applications, but also a shortcut to comprehend the growth mechanism. More importantly, unadjustable Au nanoparticle assemblies hardly accord with the concept of superparticles; intuitively understanding the growth mechanism of this structure has long-term significance for the development and application of plasmonic superparticle materials. Therefore, there is an urgent need to develop a facile, rapid synthetic method for branched Au superparticles and to regulate their optical properties by understanding the growth mechanism.

Herein, we report a facile, ultra-fast, and mass-producible fabrication method for the synthesis of branched Au superparticles by seed-mediated growth, yielding uniform and well-dispersed core–shell Au superparticles in 5 seconds at room temperature. The role of surfactants in the synthetic process is investigated through designed experiments, and the key factor of branched structure formation is the frequent toggling between layer by layer growth mode and island growth mode induced by 3-aminophenol, leading to the island-on-island growth of the Au nanoparticles. In addition, the special growth mode is due to the continuous relatively high surface energy, which is related to the synergistic effect between the amino group and the hydroxyl groups of 3-aminophenol, and the hydroxyl group provides the continuous adsorption capacity toward the growth interface. Based on the proposed mechanism, the optical properties of branched Au superparticles could be regulated by changing the core scale, branch width, and the scale of Au island-like nanoparticles. Additionally, we briefly demonstrate the excellent properties of branched Au superparticles with different morphologies, such as photothermal conversion and therapy and NIR SERS. The photothermal conversion efficiency under 1064 nm irradiation was calculated to be as high as 62.6%. This work gives insight into the growth mechanism of branched Au superparticles and provides a potential multifunctional plasmonic material for efficient NIR sensing fields.

Results and discussion

The characterization of branched Au superparticles

The synthetic process of the branched Au superparticles is shown in Fig. 1a, which is a typical seed growth method, and the Au seeds were prepared as we previously reported (see the ESI†).[15] As the reducing agents (3-aminophenol) were added into the precursor solution, the color changed from red to black in 5 seconds (please refer to the video in the ESI†), their optical photos and extinction spectra are shown in Fig. 1b; one can find that the plasmonic band of the obtained Au superparticles is obviously extended compared with the Au seeds, implying the

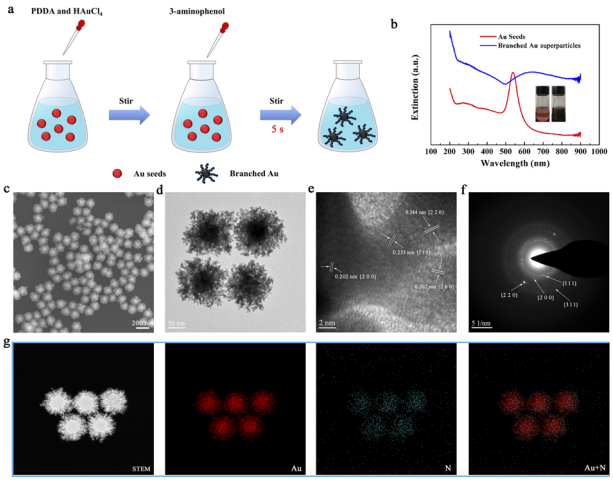

Fig. 1 (a) The synthetic strategy of branched Au superparticles. (b) The optical photos and extinction spectra of branched Au superparticles and Au seeds. (c) The SEM image, (d) TEM image, (e) HR-TEM image, (f) SAED pattern, and (g) STEM and EDX element mapping images of branched Au superparticles.

existence of multiple plasmonic coupling modes. The well-dispersed Au superparticles are core–shell structures, the core is a spherical Au seed (diameter: *ca.* 60 nm), and the branched shell consists of abundant small Au island-like nanoparticles, which is clearly illustrated by scanning electron microscopy (SEM) and transmission electron microscopy (TEM), as shown in Fig. 1c and d. According to the high-resolution transmission electron microscopy (HR-TEM) image in Fig. 1e, the Au island-like nanoparticles demonstrate a polycrystalline structure with lattice fringe widths of 0.233 nm, 0.202 nm, and 0.144 nm, which are assigned to the (1 1 1), (2 0 0), and (2 2 0) lattice planes, respectively.[16] Meanwhile, the typical multi-ring diffraction pattern of selected area electronic diffraction (SAED) of a single Au superparticle is also consistent with the HR-TEM image, as shown in Fig. 1f. The formation of the polycrystalline structure is caused by the absence of capping agent of the designated crystallographic plane.[17,18] Moreover, the branched Au superparticles are mainly composed of Au and N elements, and the nitrogen is attributed to the surfactants, which is demonstrated by scanning transmission electron microscopy (STEM) and element mapping of energy dispersive X-ray spectroscopy (EDX) (Fig. 1g). Overall, the uniformly branched Au superparticles were successfully obtained.

The growth mode of branched Au superparticles and its influential factor

Usually, there are two main types of seed-mediated growth modes of nanoparticles, one is the Frank–van der Merwe (FM) growth mode, a layer-by-layer growth mode; the other is the Volmer–Weber (VW) growth mode, an island on surface growth mode.[13,19–21] The decisive factor for the growth mode is the surface energy at the growth interface in these two modes. Generally, the surface energy of FM mode is relatively low; conversely, a higher surface energy is a prerequisite for island growth in VW mode.[14] However, the surface energy of the

growth interface could be decreased by the deposition of elements as the growth progresses.[14] Therefore, the VW mode can probably be transformed into FM mode during the growth process without supplementary surface energy. Therefore, according to the special morphology, the growth process of the branched Au superparticles might be a continuous VW mode.

Typically, there are many factors that affect the surface energy during seed-mediated growth, such as lattice mismatch, and surfactant.[13,14] However, in our work, the main influencing factor of surface energy is only the surfactant because there is no lattice mismatch and the existence of multiphase. Therefore, we will focus on the effect of surfactants on the growth mode in our case.

We systematically investigated the role of surfactants in the synthetic process through controllable experimental conditions. The TEM images of branched Au superparticles fabricated using different amounts of poly(diallyldimethylammonium)chloride (PDDA) are shown in Fig. S1.† According to Fig. S1a† (PDDA content is zero), it can be found that extensively branched self-nucleation superparticles appeared in the solution, and there are few thin branches on each seed nanoparticle. Obviously, the branched morphology still exists when PDDA is absent, indicating the negligible relationship between PDDA and relatively high surface energy. As the content of PDDA increased to more than 5 μL in the synthetic system, the phenomenon of self-nucleation obviously disappeared, and the morphology of branched Au superparticles became more uniform, which is illustrated by TEM images in Fig. S1b–d.† Furthermore, the extinction spectra of branched Au superparticles with different PDDA contents are shown in Fig. S2.† In the spectrum of superparticles without PDDA, there are two extinction peaks that are located at 560 nm (the plasmonic band of pristine seed nanoparticles located at 540 nm) and 770 nm, which are assigned to the seed nanoparticles and the self-nucleation branched superparticles, respectively. Then, as the contents of PDDA increased, the morphology of branched Au superparticles became more uniform; therefore, the two optical extinction peaks merged into one peak and gradually blue-shifted. Based on the TEM images and optical extinction spectra, PDDA is a surfactant that dynamically tunes the uniformity and stability of branched superparticles, but it is independent of the relatively high surface energy.

The TEM images of branched Au superparticles fabricated using different contents of 3-aminophenol are shown in Fig. S3;† the branched structure is very messy when the content of 3-aminophenol was 35 μL in this synthetic system, but it gradually became uniform as the content of 3-aminophenol increased. Note that the amount of 3-aminophenol cannot be zero since it is the reducing agent for this synthetic process. Moreover, their optical extinction spectra are shown in Fig. S4,† and there is an extended plasmonic band in the spectrum of Au superparticles synthesized using 35 μL of 3-aminophenol, implying the irregular structure of superparticles, which is consistent with the TEM image. As the amounts of 3-aminophenol increased, the plasmonic peaks gradually narrowed and blue-shifted, indicating that the structure became more homogeneous. Furthermore, we also employed some other reducers instead of 3-aminophenol for fabricating Au superparticles, such as ascorbic acid, dopamine, and sodium borohydride. However, none of them could achieve this branched structure (Fig. S5†), implying the close relationship between this distinctive structure and 3-aminophenol. Based on these results, it is easy to know that 3-aminophenol is not only a reducing agent but also a morphology controlling agent.

The influence of the 3-aminophenol substituent toward the growth process

To further investigate the underlying mechanism of 3-aminophenol for inducing this branched structure, we comprehensively analyzed the role of the functional groups in its molecular formula. Simply, 3-aminophenol is composed of a benzene ring, an amino group, and a hydroxyl group, and the hydroxyl group and amino group are located at the number 1 and number 3 sites of the benzene ring, respectively. First, we performed the parallel experiments by changing the position of the substituent; therefore, 2-aminophenol and 4-aminophenol were used to fabricate Au superparticles, and their corresponding TEM images are shown in Fig. 2a and c. Predictably, both of them could acquire branched structures, but their branch widths are much narrower than that of 3-aminophenol (Fig. 2b), and the degrees of polycrystallinity are also decreased, which is illustrated by the SAED patterns in the insets. Therefore, the first set of parallel experiments proved that the position of the substituent can affect the growth state of the branched structure.

Furthermore, we changed the hydroxyl group to the amino group based on the first set of parallel experiments, namely, *o*-phenylenediamine, *m*-phenylenediamine, and *p*-phenylenediamine were employed to synthesize Au nanoparticles, and their TEM images are shown in Fig. 2d–f, respectively. Interestingly,

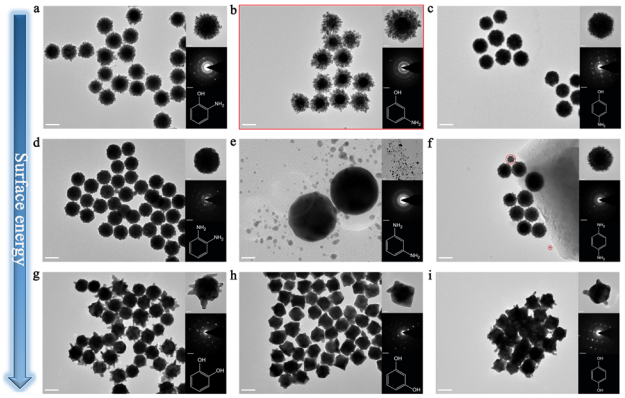

Fig. 2 (a–c) The TEM images of branched Au superparticles fabricated with 2-aminophenol, 3-aminophenol, and 4-aminophenol, respectively, in the experiments. (d–f) The TEM images of seed-mediated growth Au nanoparticles fabricated with *o*-phenylenediamine, *m*-phenylenediamine, and *p*-phenylenediamine, respectively. (g–i) The TEM images of seed-mediated growth Au nanoparticles fabricated with catechol, resorcinol, and hydroquinone, respectively. The scale bar in (e) is 20 nm, the others are 100 nm, and the scale bars in the inset are 20 nm and 5 1/nm, respectively. The SAED patterns correspond to the HRTEM images. The molecular formula in the inset corresponds to the reducing agent of each experiment.

the multi-island structure still appeared in the experiments when *o*-phenylenediamine and *p*-phenylenediamine were present, indicating that the amino group might be the origin of the relatively high surface energy. The diameter of Au island-like nanoparticles is larger than that of the first set of experiments; meanwhile, the clearer dot matrix patterns in the SAED pattern demonstrate the trend from poly-crystal to single-crystal (insets). Unexpectedly, abundant small self-nucleation Au nanoparticles appeared in the reaction involving *m*-phenylenediamine, and there is nothing on the Au seeds, despite it is just a difference of a hydroxyl group compared with 3-aminophenol (Fig. 2b). In addition, the partial self-nucleation phenomenon also appeared in the experiment of *p*-phenylenediamine, but the morphology of self-nucleation nanoparticles is still a multi-island morphology compared with the spherical morphology in an *m*-phenylenediamine experiment, which is illustrated in Fig. S6† and the inset in Fig. 2e. In contrast, there is no self-nucleation in the experiment of *o*-phenylenediamine. Generally, the binding capability of *o*-phenylenediamine with Au nanoparticles is stronger than that of other isomers according to the literature.[22] Therefore, this self-nucleation phenomenon might be caused by insufficient binding capability, and the position of groups can affect the binding capability of a molecule. Furthermore, the hydroxyl group might offer robust binding capability for surfactant molecules to Au nanoparticles, and the amino group may be the main cause of the relatively high surface energy.

Moreover, we changed the amino group to the hydroxyl group based on the second set of parallel experiments; scilicet, catechol, resorcinol, and hydroquinone were employed to synthesize Au nanoparticles, and their TEM images are shown in Fig. 2g–i. Expectedly, none of them can reproduce this branched structure that is composed of abundant small Au island-like nanoparticles, but there is no self-nucleation phenomenon in them, which is in good agreement with previous speculation. Moreover, the obvious dot matrix pattern in the insets demonstrates the formation of single-crystal during the synthesis. Therefore, the hydroxyl group is not the main cause of the relatively high surface energy, but it provides strong binding capability for surfactants with Au nanoparticles.

Moreover, the extinction spectra of Au nanoparticles of the three sets of experiments are shown in Fig. S7.† The spectra of each set are significantly different, which is in good agreement with the TEM images.

The growth mechanism of branched Au superparticles

Generally, the crystal-growth rate is exponentially correlated with the surface energy,[23] and the seed-mediated growth rate of Au nanoparticles can be considered as the reductive rate of chloroauric acid if there is no self-nucleation phenomenon. Therefore, growth rates of most of the Au nanoparticles are equal to the reductive rates of chloroauric acid except in the experiments of *m*-phenylenediamine (growth rate is zero) and *p*-phenylenediamine (growth rate is lower than the reductive rate) in our case. Meanwhile, these molecules are also reducing agents in the growth process, and thereby the surface energy might be estimated from the reductive reaction rate. Although the reductive ability of aniline is stronger than that of phenol,[24] the oxidation potential of 4-aminophenol (1.062 V) is lower than that of *p*-phenylenediamine (1.16 V) according to the literature,[25] indicating that the reductive ability of 4-aminophenol is stronger than that of *p*-phenylenediamine, despite the latter possesses an additional amino group, which might be caused by the synergistic effect between the amino group and hydroxyl group. Therefore, as the reaction rates of synthesis gradually decreased from the first set experiment to the third set, the quantities of small islands in the Au nanoparticle shell also decreased, and the scales of islands increased, which is caused by the more growth time of FM mode due to the insufficient surface energy, implying that the surface energy is decreased as the reaction rate decreased. In addition, the trend from poly-crystal to single-crystal might also be caused by this transformation of surface energy. Consequently, based on the parallel experiments, the relatively high surface energy during the synthesis process is related to the special structure of 3-aminophenol, the amino groups combined with hydroxyl groups to supply the relatively high surface energy, and the hydroxyl groups provide the robust binding capability, ensuring its continuous and rapid adsorption on the surface of Au atoms, leading to sustained supplementation of surface energy.

According to the above analysis, we can expatiate the growth mechanism of branched Au superparticles in detail. First, the newborn Au atoms are deposited on the surface of Au seeds through layer-by-layer mode (FM mode) when the reductive reaction begins; yet this process is transient because abundant 3-aminophenol rapidly binds to the surface of Au atoms leading to relatively high surface energy, and FM mode transforms into the VW mode. Then, multiple heterogeneous nucleation sites appear on the surface of the seeds, on which newborn Au atoms are selectively deposited. The surface energy decreases as the deposition of Au atoms, the VM mode is transformed into the FM mode again, and these nucleation sites gradually grow into islands *via* a layer-by-layer mode. When the diameter of Au island-like nanoparticles increases to several nanometers, the surface energy exceeds the threshold *via* the cumulative adsorption of 3-aminophenol; therefore, the FM mode transforms into VW mode once again, and multiple heterogeneous nucleation sites appear in the Au island-like nanoparticles. Immediately, the growth continues to repeat the above process. Finally, the island-on-island branched structure is obtained by the multiple above-mentioned looping processes.

The morphology regulation of the branched Au superparticles

Based on the proposed mechanism, we can know that the diameter of Au island-like nanoparticles is related to the growth time of each FM mode. Therefore, modulating the reaction rate or the binding capability of 3-aminophenol is an efficient method to regulate the scale of each island nanoparticle. Since the aqueous solution of 3-aminophenol is alkaline, thus we attempted to regulate its reducing rate *via* hydrochloric acid (HCl). Consequently, the TEM images of branched Au superparticles fabricated with different amounts of HCl and their

extinction spectra are shown in Fig. S8 and S9.† Unfortunately, the morphology of branched Au superparticles was almost unchanged at low concentrations of HCl, and obvious etching of Au seeds occurred as the concentrations of HCl increased, indicating that the reducing ability of 3-aminophenol is independent of the pH value. Furthermore, their extinction spectra were in good agreement with the morphologies, and the curves were almost unchanged at low concentrations of HCl and gradually blue-shifted with the increase of concentrations.

Additionally, cetyltrimethylammonium chloride (CTAC) is also a general surfactant to adjust the reaction rate of seed-mediated growth, and they could combine with Au ions to form complexes that indirectly reduce the reaction rate.[26,27] Therefore, as an extra surfactant, different concentrations of CTAC were introduced to synthesize branched Au superparticles, and their TEM images are shown in Fig. 3a–e. Expectedly, the diameter of Au island-like nanoparticles of branched Au superparticles gradually increased as the amount of CTAC increased from 0 to 400 μL in the synthetic system, and the diameters of islands and widths of branches are counted in Fig. 3f. The diameters of islands are 4.83 ± 1.03 nm, 7.43 ± 1.68 nm, 7.66 ± 1.28 nm, 9.2 ± 2.37 nm, and 10.9 ± 1.69 nm, respectively; the widths of branches are 39.3 ± 11.8 nm, 28.9 ± 3.6 nm, 22.8 ± 6.4 nm, 22.3 ± 4.2 nm, and 19.8 ± 3.2 nm, respectively.

Moreover, their plasmonic peak locations also gradually red-shifted as the amount of CTAC increased, and the extinction spectra are shown in Fig. S10.† Nevertheless, the uniformity of branched Au superparticles is disturbed, which is caused by the competitive adsorption between CTAC and 3-aminophenol, although it is also a method to regulate the surface energy of synthesis.

Furthermore, we successfully regulated the width of the branch of Au superparticles by controlling the amount of chloroauric acid, and their TEM images and extinction spectra are shown in Fig. S11 and S12.† Briefly, the width of the branch is proportional to the content of chloroauric acid, and the plasmonic band broadened gradually with increasing chloroauric acid contents.

Therefore, we can well regulate the morphology of branched Au superparticles by tuning the scale of Au island-like nanoparticles, the width of the branch, and the scale of Au seeds.

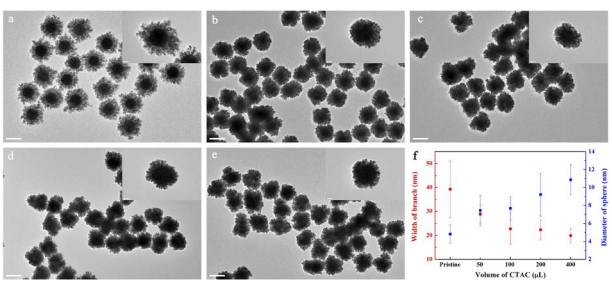

Fig. 3 (a–e) The TEM images of branched Au superparticles with different CTAC contents ((a) is 0 μL, (b) is 50 μL, (c) is 100 μL, (d) is 200 μL and (e) is 400 μL, the concentration is 0.1 M). The scale bars are 100 nm, and the scale bars in the inset are 20 nm. (f) The statistics of branched widths and island diameters of branched Au superparticles.

Furthermore, the synthetic method could easily magnify ten times to fabricate the branched Au superparticles, which is illustrated by the video in ESI.†

Additionally, we compare the synthetic results of Au superparticles with the data from the literature,[14,28–31] which is shown in Table S1.† It can be found that our method is not only facile and efficient but also more uniform in the morphology of superparticles. More importantly, our work provides a complete explanation of the morphological evolution of Au nanoparticles from heterogeneous core–shell particles to superparticles and reveals the key factors of the growth process of Au superparticles, providing important insight for the synthesis of noble metal superparticles.

Diversified NIR optical sensing applications of branched Au superparticles

Usually, the optical properties of Au nanoparticles are related to their morphology. Consequently, the branched Au superparticles could be applied to several optical sensing fields *via* the above-mentioned adjustments. Generally, the extinction of plasmonic nanoparticles consists of absorption and scattering. Most of the optical energy absorbed by the nanoparticles can be transformed into heat by the generation of phonons,[32] and thereby the plasmonic nanoparticles can be used for photothermal conversion. As the smaller nanoparticles possess the higher absorption proportion in extinction,[32] thus we selected the Au seeds with a diameter of approximately 40 nm to fabricate branched Au superparticles for the measurement of photothermal conversion. Therefore, the heating curves of different concentrations of pristine branched Au superparticles (without CTAC) aqueous solution under 1064 nm laser irradiation (1 W cm^{-2}) are shown in Fig. 4a. Compared with aqueous solution, the temperature of pristine Au superparticle solutions increased significantly with increasing time, and the heating trend of the higher concentration ones is sharper. The temperature of 100 ppm solution was risen to be as high as 63.4 °C after 10 min of irradiation. Note that the volume of Au superparticles solution used for photothermal conversion is 1 mL, which is larger than the average level in the literature;[3,14,31,33] the concentrations of superparticles solution were confirmed by inductively coupled plasma mass spectrometry (ICP-MS). The extinction spectra of different concentrations of pristine Au superparticles are shown in Fig. 4b. The strong extinction is extended from 400 nm to 1200 nm, exhibiting blackbody-like extinction. The photothermal conversion efficiency (PCE) was calculated to be as high as 62.6%; the heating and cooling curves are shown in Fig. 4c. In addition, the PCE properties of branched Au superparticles fabricated with 400 μL CTAC were also measured, and their graphics are shown in Fig. 4d–f. In contrast, they are weaker than pristine superparticles (without CTAC) both in the heating temperature and extinction coefficient, and their PCE was calculated to be 40.5%, demonstrating that the coupling of more and smaller Au island-like nanoparticles is propitious to optical absorption.

Additionally, surface-enhanced Raman spectroscopy is also a general application for plasmonic nanoparticles, which is based on the surface-enhanced Raman scattering effect of

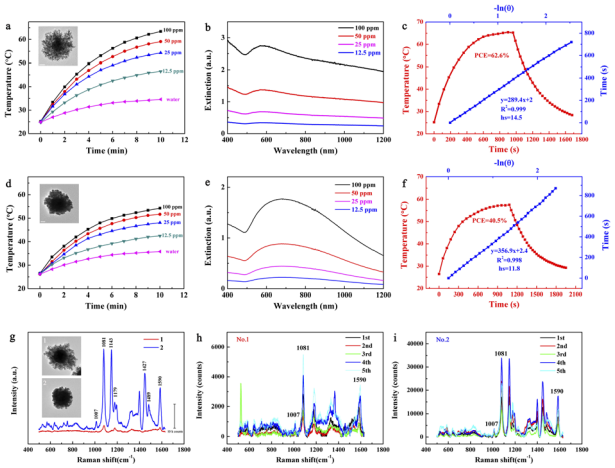

Fig. 4 (a) Temperature curves of pristine branched Au superparticles (without CTAC) solution with different concentrations under 1064 nm laser irradiation (1 W cm^{-2}). Inset is the morphology of branched Au superparticles. (b) Extinction spectra of pristine Au superparticles with different concentrations. (c) Calculation of photothermal conversion efficiency at 1064 nm. The red dots are the heating and cooling curves of pristine Au superparticle solution. Blue dots show the time constant (τ_s) for the heat transfer from the system determined by applying the linear time data from the cooling period. (d–f) The PCE properties of branched Au superparticles fabricated with 400 μL CTAC, these graphics correspond to (a), (b), and (c), respectively. (g) The SERS spectra of 4-ATP based on the different substrates, 1 refers to the pristine branched Au superparticles (without CTAC), 2 refers to the branched Au superparticles fabricated with 400 μL CTAC. (h) The multiple test SERS spectra of 4-ATP based on substrate 1. (i) The multiple test SERS spectra of 4-ATP based on substrate 2.

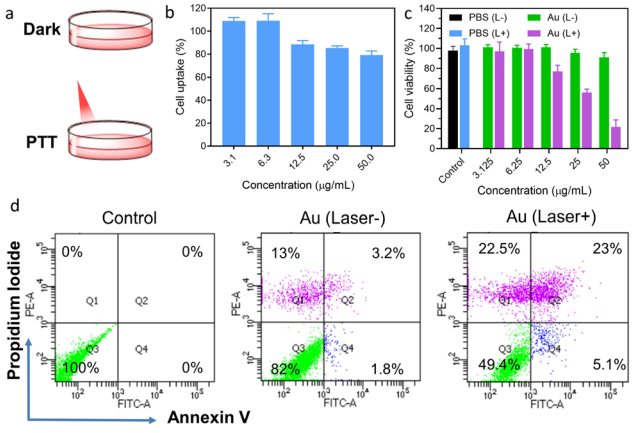

Fig. 5 (a) The scheme of *in vitro* photothermal therapy (PTT). (b) The cell uptake measurement of pristine branched Au superparticles. (c) The cytotoxicity measurement of PTT treatment. + refers to the laser turn on, − means the laser turn off. (d) The cell apoptosis induced by PTT treatment. Q1 refers to the ratio of necrotic cells, Q2 refers to the cell ratio of late-stage apoptosis, Q3 is the ratio of live cells, and Q4 is the cell ratio of early apoptosis. The μg mL^{-1} is equal to the ppm, and the wavelength of the laser is 1064 nm.

them, and NIR SERS has attracted much attention currently due to its good signal anti-interference capability and tissue penetration capability.[20,34] Obviously, SERS is related to the scattering in their extinction and thereby the larger nanoparticles are suited to the SERS because of the more scattering proportion in extinction.[32] In addition, the matching between extinction peaks and the wavelength of the laser is also an important factor for the SERS test. Therefore, these two kinds of branched Au superparticles (with a core diameter of 60 nm) were also subjected to the SERS measurements (Fig. 4g). Typically, 10^{-6} M 4-aminothiophenol (4-ATP) was used as a model molecule for the SERS test; the wavelength of the laser was 785 nm. In contrast, the pristine superparticles without CTAC exhibit poor SERS signal intensity while the intensity of superparticles fabricated with 400 μL CTAC is much stronger than the former. Several repeated measurements are shown in Fig. 4h and i. It can be found that the signal intensity gap between the two kinds of superparticles is still large despite a certain intensity fluctuation, indicating that the larger scale of Au island-like nanoparticles is more suitable for SERS application.

Moreover, the pristine Au superparticles (without CTAC) were also employed for the measurement of *in vitro* NIR-II photothermal therapy (PTT); the PTT process is shown in Fig. 5a. According to the cell uptake results in Fig. 5b, the cell uptake ratio slightly decreased as the concentrations of superparticles increased; the still approximately 80% cell uptake ratio under 50 ppm superparticles indicates that the cells possess good uptake of superparticles. Moreover, the cytotoxicity of superparticles was measured, as shown in Fig. 5c. The excess 90% cell viability in the dark at different concentrations of superparticles indicates the high biocompatibility of these branched Au superparticles. Compared with almost 100% cell viability in PBS solution, the superparticle solution exhibits a high cell death ratio under 1064 nm laser irradiation (1 W cm^{-2}, 5 min); the cell death ratio in the 50 ppm superparticle solution is approximately 80%, which is stronger than that of Au nanorods and equivalent to the current excellent photothermal agents.[35–38] Moreover, the apoptosis induced by PTT treatment was measured by flow cytometry using a cell apoptosis kit; the results are shown in Fig. 5d. About 18% (13% is necrotic cells, refers to the Q1 value) cell death occurred in the cells treated with superparticles in a dark environment, which agrees with the cell viability results. As the laser was turned on, the cell death ratio increased to 50.6%, most of which were early apoptosis and late-stage apoptosis (Q2 and Q4), indicating the good PTT efficiency of superparticles. Moreover, we compare the PCE value of Au superparticles with the data of Au nanoparticles from the literature (Table S2†).[3,39–43] To the best of our knowledge, the best NIR-II PCE value of pure-gold nanomaterials is no more than 70% currently, combined with the good PTT effect *in vitro* as above; therefore, our branched Au superparticles are excellent PTT materials.

Overall, the above measurements exhibit the performance advantages and potential applications of branched Au superparticles with different morphologies.

Conclusions

In summary, a facile ultra-fast and tunable synthesis method of branched Au superparticles is developed, and uniform and well-

dispersed superparticles were prepared in 5 seconds at room temperature by a chemical route induced by 3-aminophenol. These superparticles are core–shell structures, the core is a Au spherical nanoparticle, and the shell is a branched structure consisting of multiple small Au island-like nanoparticles. The formation mechanism is systematically investigated by controlled variable experiments on the functional groups of 3-aminophenol. We reveal that the special growth mode is due to the relatively high surface energy caused by the synergistic effect between amino groups and hydroxyl groups, as well as the strong binding capability toward growth interface originated from hydroxyl groups. We further confirm the toggling formation mechanism of Au superparticles between the FM growth mode and the VW growth mode induced by 3-aminophenol. Based on it, the morphology of branched Au superparticles could be well regulated by controlling the scale of Au island-like nanoparticles, the width of branches, and the diameter of Au seeds. The as-prepared Au superparticles demonstrate a broadband absorption from visible to near-infrared regions due to their multiple plasmonic coupling and hence they have important applications in sensors, photothermal conversion and therapy, *etc.* We also exhibit their multifunctional applications corresponding to the different morphologies of branched Au superparticles in photothermal conversion, SERS. The photothermal conversion efficiency under 1064 nm laser irradiation was calculated to be as high as 62.6%. They exhibit an outstanding *in vitro* photothermal therapy effect. This work provides an insight into the growth mechanism of branched Au superparticles and provides an important broadband absorption material for highly efficient optical applications.

Conflicts of interest

There are no conflicts to declare.

Acknowledgements

The authors acknowledge the financial support from the National Science Fund for Distinguished Young Scholars (Grant No. 51825103), the Natural Science Foundation of China (Grant No. 52171232, 52201232, and 52001306), the Youth Innovation Promotion Association of Chinese Academy of Sciences (Grant No. 2022449), and the Scientific Instrument Developing Project of the Chinese Academy of Sciences, Grant No. YJKYYQ20210009.

Notes and references

1 J. Zheng, X. Cheng, H. Zhang, X. Bai, R. Ai, L. Shao and J. Wang, *Chem. Rev.*, 2021, **121**, 13342–13453.
2 J. Lu, Y. Xue, K. Bernardino, N.-N. Zhang, W. R. Gomes, N. S. Ramesar, S. Liu, Z. Hu, T. Sun, A. F. de Moura, N. A. Kotov and K. Liu, *Science*, 2021, **371**, 1368–1374.
3 J. Jia, G. Liu, W. Xu, X. Tian, S. Li, F. Han, Y. Feng, X. Dong and H. Chen, *Angew. Chem., Int. Ed.*, 2020, **132**, 14551–14556.
4 G. González-Rubio, J. Mosquera, V. Kumar, A. Pedrazo-Tardajos, P. Llombart, M. Solís Diego, I. Lobato, G. Noya Eva, A. Guerrero-Martínez, M. Taboada José, F. Obelleiro, G. MacDowell Luis, S. Bals and M. Liz-Marzán Luis, *Science*, 2020, **368**, 1472–1477.
5 J. Wang, X. Wu, W. Ma and C. Xu, *Adv. Funct. Mater.*, 2020, **30**, 2000670.
6 W. Zhang, Q. Li and M. Qiu, *Opt. Express*, 2013, **21**, 172–181.
7 J. Huang, C. Liu, Y. Zhu, S. Masala, E. Alarousu, Y. Han and A. Fratalocchi, *Nat. Nanotechnol.*, 2016, **11**, 60–66.
8 T. Wang, D. LaMontagne, J. Lynch, J. Zhuang and Y. C. Cao, *Chem. Soc. Rev.*, 2013, **42**, 2804–2823.
9 D. Liu, F. Zhou, C. Li, T. Zhang, H. Zhang, W. Cai and Y. Li, *Angew. Chem., Int. Ed.*, 2015, **54**, 9596–9600.
10 Y. Wang, O. Zeiri, M. Raula, B. Le Ouay, F. Stellacci and I. A. Weinstock, *Nat. Nanotechnol.*, 2017, **12**, 170–176.
11 J. H. Yu, M. S. Jeong, E. O. Cruz, I. S. Alam, S. K. Tumbale, A. Zlitni, S. Y. Lee, Y. I. Park, K. Ferrara, S. H. Kwon, S. S. Gambhir and J. Rao, *ACS Nano*, 2023, **17**, 2554–2567.
12 N. Kwon, H. Oh, R. Kim, A. Sinha, J. Kim, J. Shin, J. W. M. Chon and B. Lim, *Nano Lett.*, 2018, **18**, 5927–5932.
13 F.-R. Fan, D.-Y. Liu, Y.-F. Wu, S. Duan, Z.-X. Xie, Z.-Y. Jiang and Z.-Q. Tian, *J. Am. Chem. Soc.*, 2008, **130**, 6949–6951.
14 Q. Zhong, J. Feng, B. Jiang, Y. Fan, Q. Zhang, J. Chen and Y. Yin, *J. Am. Chem. Soc.*, 2021, **143**, 20513–20523.
15 T. Zhang, X. Li, C. Li, W. Cai and Y. Li, *Chem. Mater.*, 2021, **33**, 2593–2603.
16 J. D. Hanawalt, H. W. Rinn and L. K. Frevel, *Ind. Eng. Chem., Anal. Ed.*, 1938, **10**, 457–512.
17 Y. Xia, Y. Xiong, B. Lim and S. E. Skrabalak, *Angew. Chem., Int. Ed.*, 2009, **48**, 60–103.
18 Y. Xia, X. Xia and H. C. Peng, *J. Am. Chem. Soc.*, 2015, **137**, 7947–7966.
19 J. Feng, D. Xu, F. Yang, J. Chen, C. Wu and Y. Yin, *Angew. Chem., Int. Ed.*, 2021, **60**, 16958–16964.
20 G. Wang, Y. Liu, C. Gao, L. Guo, M. Chi, K. Ijiro, M. Maeda and Y. Yin, *Chem*, 2017, **3**, 678–690.
21 P. Zeng, L. Hang, G. Zhang, Y. Wang, Z. Chen, J. Yu, T. Zhang, W. Cai and Y. Li, *Small*, 2022, **18**, 2204748.
22 Y.-L. Li, Y.-M. Leng, Y.-J. Zhang, T.-H. Li, Z.-Y. Shen and A.-G. Wu, *Sens. Actuators, B*, 2014, **200**, 140–146.
23 Y. W. Jun, J. S. Choi and J. Cheon, *Angew. Chem., Int. Ed.*, 2006, **45**, 3414–3439.
24 E. Bendary, R. R. Francis, H. M. G. Ali, M. I. Sarwat and S. El Hady, *Ann. Agric. Sci.*, 2013, **58**, 173–181.
25 J. D. S. Newman and G. J. Blanchard, *Langmuir*, 2006, **22**, 5882–5887.
26 M. L. Personick and C. A. Mirkin, *J. Am. Chem. Soc.*, 2013, **135**, 18238–18247.
27 T. Zhang, X. Li, Y. Sun, D. Liu, C. Li, W. Cai and Y. Li, *Chem. Sci.*, 2021, **12**, 12631–12639.
28 L. Tian, S. Tadepalli, M. Fei, J. J. Morrissey, E. D. Kharasch and S. Singamaneni, *Chem. Mater.*, 2015, **27**, 5678–5684.
29 P. Qiu, M. Yang, X. Qu, Y. Huai, Y. Zhu and C. Mao, *Biomaterials*, 2016, **104**, 138–144.
30 Y. Shao, W. Xu, Y. Zheng, Z. Zhu, J. Xie, X. Wei, Y. Zhang, J. Zhang, Q. Wu, J. Wang and Y. Ding, *Chem. Eng. J.*, 2023, **455**, 140586.

31 J. Zhou, Y. Jiang, S. Hou, P. K. Upputuri, D. Wu, J. Li, P. Wang, X. Zhen, M. Pramanik, K. Pu and H. Duan, *ACS Nano*, 2018, **12**, 2643–2651.
32 J. Chen, Z. Ye, F. Yang and Y. Yin, *Small Sci.*, 2021, **1**, 2000055.
33 H. Ma, Z. Liu, Y. Wei and L. Jiang, *Colloids Surf., A*, 2019, **582**, 123889.
34 J. J. Li, C. Wu, J. Zhao, G. J. Weng, J. Zhu and J. W. Zhao, *Spectrochim. Acta, Part A*, 2018, **204**, 380–387.
35 T. He, C. Jiang, J. He, Y. Zhang, G. He, J. Wu, J. Lin, X. Zhou and P. Huang, *Adv. Mater.*, 2021, **33**, 2008540.
36 P. Vijayaraghavan, C. H. Liu, R. Vankayala, C. S. Chiang and K. C. Hwang, *Adv. Mater.*, 2014, **26**, 6689–6695.
37 W. Liu, Y. Wang, Y. Wang, X. Li, K. Qi, J. Wang and H. Xu, *ACS Appl. Mater. Interfaces*, 2022, **15**, 236–248.
38 D. Zhu, Y. Liu, M. Liu, X. Liu, P. N. Prasad and M. T. Swihart, *J. Mater. Chem. B*, 2020, **8**, 5491–5499.
39 Q. Li, L. Hang, W. Jiang, J. Dou, L. Xiao, X. Tang, Y. Yao and Y. Wang, *Biomaterials*, 2020, **257**, 120235.
40 Z. Yang, X. Ding and J. Jiang, *Nano Res.*, 2016, **9**, 787–799.
41 X. Ding, C. H. Liow, M. Zhang, R. Huang, C. Li, H. Shen, M. Liu, Y. Zou, N. Gao, Z. Zhang, Y. Li, Q. Wang, S. Li and J. Jiang, *J. Am. Chem. Soc.*, 2014, **136**, 15684–15693.
42 W. Tang, Z. Dong, R. Zhang, X. Yi, K. Yang, M. Jin, C. Yuan, Z. Xiao, Z. Liu and L. Cheng, *ACS Nano*, 2019, **13**, 284–294.
43 C. Zhang, D. Men, T. Zhang, Y. Yu, J. Xiang, G. Jiang and L. Hang, *ACS Appl. Mater. Interfaces*, 2020, **12**, 2152–2161.